PHYSICAL REVIEW B VOLUME 25, NUMBER 10 15 MAY 1982

Compton-scattering study of trigonal, monoclinic, and amorphous phases of Se

P. Krusius
Electron Physics Laboratory, Helsinki University of Technology, SF-02150 Espoo 15, Finland, and Semiconductor Laboratory, Technical Research Center of Finland, SF-02150 Espoo 15, Finland

P. Pattison and J. R. Schneider
Hahn-Meitner-Institut für Kernforschung, Postfach 39 01 28, D-1000 Berlin 39, Federal Republic of Germany

B. Kramer
Physikalisch-Technische Bundesanstalt, Bundesallee 100, D-3300 Braunschweig and Universität Dortmund, Institut für Physik, Postfach 500 500, D-4600 Dortmund 50, Federal Republic of Germany

W. Schülke, U. Bonse, and J. Treusch
Universität Dortmund, Institut für Physik, Postfach 500 500, D-4600 Dortmund 50, Federal Republic of Germany

(Received 20 January 1981; revised manuscript received 21 July 1981)

The Compton profiles (CP) and autocorrelation functions (AF) for crystalline trigonal Se (*t*-Se), polycrystalline trigonal Se (pct-Se), polycrystalline monoclinic Se (pcm-Se), and black amorphous Se (ba-Se), have been determined experimentally from inelastic γ-ray scattering. Two different γ-ray spectrometers have been used, namely one using the 412-keV line of ^{198}Au and the other using the 59.5-keV line of ^{241}Am. The momentum resolutions were 0.41 and 0.56 a.u., respectively. The present results for *t*-Se, pct-Se, and ba-Se differ significantly from earlier results. The data are analyzed using theoretical results obtained from atomic restricted Hartree-Fock models, free-electron (FE) models, one-dimensional potential array studies, and from self-consistent orthogonalized-plane-wave (SCOPW) calculations based on a local density formalism. Good agreement for *t*-Se and pct-Se has been obtained between both sets of experimental data and the SCOPW results. The FE model, fulfilling the correct translation symmetry and occupation of the higher Brillouin zones, is shown to explain long-range oscillations of the AF qualitatively but is inadequate for describing the short-range bonding effects. No significant difference within the present resolution was detected between the CP and the AF of pct-Se and ba-Se, contrary to earlier findings. Reasons for this are discussed using the above models. A significant difference between pct-Se and pcm-Se has not been obtained with the Am spectrometer.

I. INTRODUCTION

In photon Compton scattering, incident photons are inelastically scattered from electrons and thus shifted to a lower energy. The motion of electrons gives rise to a broadening of the Compton line and therefore the analysis of the line shape yields information on the velocity distribution of the scattering electrons. In order to facilitate the analysis of the process, the energy of the incident monochromatic photons is usually limited to the hard x- or γ-ray regimes and the scattering angle close to 180°.[1] As a consequence the scattered electrons are promoted into free-particle states and hence, the scattering cross section only depends on the initial state of the electrons. This is the impulse approximation[2] (IA), the validity of which has been assessed for the hydrogen atom,[3] and is currently used for the analysis of Compton spectra of many electron systems, i.e., for atoms, molecules, and solids.

Within the IA the scattering cross section is pro-

 ©1982 The American Physical Society

portional to the Compton profile (CP),

$$J_{\vec{k}}(q)=\int dp^3\Gamma_1(\vec{p},\vec{p})\delta(q-\vec{p}\cdot\vec{k}/k)\ , \qquad (1)$$

where $\vec{k}$ denotes the scattering vector and Γ_1 the one-electron density matrix. The CP depends only on the ground-state momentum density $\Gamma_1(\vec{p},\vec{p})$ of the electrons. The Fourier-transformed CP is a position-space quantity and may be written as

$$B(\vec{t})=\int dr^3\Gamma_1(\vec{r},\vec{r}+\vec{t}),\quad \vec{t}\,||\,\vec{k}\ , \qquad (2)$$

the autocorrelation function (AF). Because of the direct relation to Γ_1, or equivalently in the independent particle model to the one-electron wave functions, Compton spectroscopy has been widely used to study various properties of Γ_1 for atoms,[4] molecules,[5] and solids.[6]

The motivation for the present study is the following. Compton studies of phase differences for the covalent semiconductor Se (Ref. 7) suggest the existence of a large difference between the spectra of polycrystalline trigonal Se (pct-Se) and black amorphous Se (ba-Se). According to simple atomic[8] and solid-state models,[9] these data were consistent with a more atomiclike momentum density in the amorphous phase. Subsequent analysis of AF (Ref. 10) in comparison with crystalline trigonal Se (*t*-Se) results, obtained from a self-consistent orthogonalized-plane-wave (OPW) study[11] based on the local density formalism, suggested a possible difference in the electronic ground state between the ba-Se and pct-Se phases at distances beyond the nearest neighbor. This was in contrast to both the radial distribution functions from elastic x-ray scattering[12] and to a one-dimensional-model study of ordered and disordered potential arrays.[13] Reexamination of the experimental data-processing procedure led to the discovery of some computational errors which occurred in the processing of the Se data. In addition, there were hints of nitrogen contamination of the amorphous Se sample. Therefore, we have started a completely new experimental and theoretical investigation in order to clarify the above discrepancies. New amorphous samples were used, which were prepared by quenching in an evacuated quartz tube in order to avoid contamination problems.

The outline of the paper is the following. In Sec. II experimental aspects and sample preparation are described. In Sec. III we give a brief description of the theoretical models used. The results for the crystalline polycrystalline and amorphous phases are given in Secs. IV–VI. A discussion of the relation between the resolution of the present Compton spectrometers and chemical bonding in covalent semiconductors follows with specific results for Se.

II. EXPERIMENT

In the Compton spectrometer operating at the Hahn-Meitner-Institut (HMI), a ^{198}Au γ-ray source provides incident photons with a strong, isolated gamma line at 412 keV. The source strength at the beginning of the measuring period is approximately 200 Ci, and it has a half-life of 2.7 days. The measuring time for each profile was about one week, i.e., two half-lives of the source. A general review of the experimental technique is available,[14] while the present apparatus and data-processing procedure has been described in detail earlier.[15,16] Briefly, the incident, monochromatic radiation from the γ-ray source is scattered by the target through an angle of 165° into an intrinsic Ge solid-state detector. The scattered photons have an energy distribution which peaks around 160 keV and an initial intensity, in the present experiment, of about 100 counts/sec. The combined effects of the detector energy resolution and the beam divergence lead to a full width at half maximum (FWHM) of 0.41 a.u. of momentum. A total of about 2×10^7 counts were collected for each profile. The ratio of the total Compton-scattered intensity to the total background in the energy range between 140 and 180 keV was 100:1 in each case. The number of counts per channel in the peak of each profile was about 10^5, corresponding to a statistical accuracy of 0.3% in $J(0)$ and 0.5% in the difference profile $\Delta J(0)$.

The raw data were subjected to a number of correction procedures.[15,16] A measured background was subtracted, and corrections made for the detector efficiency, absorption in the sample, and the transformation from the energy spectrum to Compton profile. A deconvolution was made to remove the effects of asymmetry in the experimental resolution function, which is replaced by a Gaussian function of the same FWHM. Because of low-energy contamination of the incident energy spectrum (due to self-scattering in the gamma source itself), only the high-energy side of the experimental profile is compared with the theoretical results. The profiles were normalized to the number of electrons in the unit cell (102), which corresponds to an area of 39.815 in the momentum range 0–5 a.u. (as derived from the relativistic

free atom profiles by Biggs *et al.*[17]). A Monte Carlo procedure[18] was employed to remove the effects of multiple scattering from the experimental profiles obtained at the HMI. The resulting experimental profiles can then be compared with theory, provided the effects of the Gaussian resolution are properly taken into account.

In the spectrometer used at the University of Dortmund (UDO) (Ref. 19) an annular ^{241}Am source provides photons with a primary energy of 59.5 keV. The source strength is 1 Ci. The scattering vector varies on a cone with a mean aperture of about 2.5° around a scattering angle of 175°. An intrinsic Ge detector (Princeton Gamma IG 105) was used. The peak-to-background ratio was 100:1 (for 1 mm Al), the momentum resolution was 0.56 a.u. FWHM for pct-Se, ba-Se, and pcm-Se; and 0.65 a.u. FWHM for *t*-Se. The momentum resolution was determined from the experimental data using the FWHM of the elastically scattered line. The influence of scattering vector variations on the resolution could be neglected.[19] Different values of the FWHM of the resolution functions are due to small electronic shifts of the detector system during long-time measurements. The initial intensity was about 5 counts/sec (for 1 mm Al). Peak count and total count for pct-Se and ba-Se were 0.6×10^5 and 3.2×10^6; and for the other phases (pcm-Se, *t*-Se), 0.3×10^5 and 1.6×10^6, respectively. The peak to background ratios were 40:1, 40:1, 50:1, and 25:1 for pct-Se, ba-Se, pcm-Se, and *t*-Se, respectively.

As in the procedure of the HMI the raw data were corrected for background and sample absorption. A deconvolution was made to account for the asymmetry of the detector resolution function, and the data were corrected for the relativistic cross section. Multiple-scattering effects were removed using a Monte Carlo procedure.[18] Normalization was achieved by fitting the area of the experimental profiles, in the momentum range from 0—5 a.u. of the high-energy side of the profile, to the free-atom CP with the configuration $2s^2 2p^6 3s^2 3p^6 3d^{10} 4s^2 4p^4$, which was calculated using Clementi wave functions.[20] The $1s^2$ electrons do not contribute to the high-energy side of the CP. Profiles for all phases have been normalized to the basic structural unit with three atoms. In contrast to the HMI experiment the point $q=0$ has been fixed by the requirement that the AF has its first zeros symmetrically at $t=\pm t_1$, where t_1 denotes the first lattice translation in that direction. As long as we were only interested in profile differences (pct-Se, ba-Se, pcm-Se) the final profiles are averages of high- and low-energy sides of the CP in order to improve the statistics. If one wants to compare experimental profiles with theoretical calculations as in the case of *t*-Se, only the high-energy side of the experimental CP was used in order to be less influenced by the low-energy contamination of the primary spectrum.

The preparation of Se samples is complicated because of the existence of many solid phases with different molecular units. The *t*-Se material was obtained using the Bridgeman-Keezer technique.[21] A selected *t*-Se sample had the rectangular dimensions $10\times12\times13$ mm^3 and the face 10×12 mm^2 cut perpendicular to the *c* axis or the [001] directions.[22] The 10×13 mm^2 face was perpendicular to the *a* axis, i.e., [100]. To minimize multiple-scattering effects two thinner composite samples of *t*-Se were prepared from smaller crystals. Both had a face area of about 1 cm^2 and a thickness of 1.3 mm. For further reference these samples will be denoted *t*-Se [001] and *t*-Se [100] according to their face normals. pct-Se samples were obtained by annealing 5*N* Se powder in an evacuated quartz tube at 205 °C for 19 h and then by using high pressure to form the material into discs without any supporting agent. The two prepared samples, pct-Se$_{\rm I}$ and pct-Se$_{\rm II}$, both had a diameter of 32 mm. The sample thicknesses were 2.4 and 1.35 mm^2, respectively. The structure was checked using x-ray diffraction. For ba-Se the same starting material as for pct-Se was used. The powder was melted in an evacuated quartz tube and then quenched in liquid nitrogen. Next the material was pulverized in a mortar and finally pressed into circular disc form. The dimensions of the samples ba-Se$_{\rm I}$ and ba-Se$_{\rm II}$ were the same as for pct-Se$_{\rm I}$ and pct-Se$_{\rm II}$, respectively. X-ray diffraction provided a final check. The density defect with respect to pct-Se did not exceed 0.3%. pcm-Se was prepared from a supersaturated solution of ba-Se in CS_2 via cooling.[23] The fine-grain polycrystalline material thus obtained contained the α and β forms of monoclinic Se roughly in equal proportion. One circular disc with a diameter of 32 mm and a thickness of 0.8 mm was pressed. No other phases could be detected in x-ray diffraction. With pct-Se as a reference for the density, no defect was detectable.

III. THEORY

Most of the theoretical models used for the interpretation have been discussed at length else-

where and therefore only some essentials are listed here. The atomic models are based on restricted Hartree-Fock (RHF) orbitals in the Slater-type orbital (STO) basis.[20] The integrals for the momentum density may be done analytically for STO's and there remains one numerical integral to be performed for the CP over a smooth function. RHF CP's and AF's are thus almost of equal quality as the original RHF solution.

For the crystalline trigonal phases a model[11] resulting from a symmetrized version of the self-consistent OPW (Ref. 24) (SCOPW) method based on the local-density formalism is used. The $X\alpha$ exchange-correlation potential has been used in the effective one-electron equation. No information in addition to lattice data is taken from the experiment, and the SCOPW models contain no further adjustable parameters. The convergence properties of this method, as measured by the convergence of the Fourier transform of the effective crystal potential, have been discussed elsewhere.[25] For the CP and the AF the essential factors influencing the accuracy are the OPW convergence of the state $|n\vec{k}\rangle$ at a general $\vec{k}$ point, the cutoff radius of the momentum space for the valence states in the projection procedure, and finally the least-squares interpolation technique in the irreducible wedge of the first Brillouin zone. The associated numerical integrals are of minor importance because of the smooth nature of the ground-state quantities involved. The convergence error of the momentum density for $p < p_F$, where p_F denotes the Fermi momentum, has been estimated to be smaller than 0.5%. The inaccuracies of the two other steps are more difficult to assess, but some estimates of the overall accuracy (including also the numerical integrals) may be obtained from the test $B(\vec{T})=0$, where $\vec{T}$ is any nonzero lattice translation.[10] The relative errors of the positions of the first two zeros along the c and a axes at c, $2c$, a, and $2a$ were 0.4, 0.8, 0.3, and 2.6%, respectively. However, in these directions for $t > 2c$ and $t > 2a$, we found $|B(t)| < 0.003B(0)$ and $|B(t)| < 0.0005B(0)$, respectively. Therefore, the numerical accuracy of the SCOPW CP's and AF's seems rather satisfactory.

In order to model pure structural effects in the CP and AF we use free-electron (FE) models, of which there are several possibilities. The simplest is the isotropic FE (IFE) model with the Fermi momentum p_F defined such that the volume of the Fermi sphere equals the total volume of the occupied Brillouin zones (BZ) in the extended representation. For the IFE one has simply

$$B(t)=\frac{6n}{(p_F t^2)}\frac{\sin(p_F t)}{(p_F t)-\cos(p_F t)}\,, \tag{3}$$

where n denotes the number of filled valence bands ($n=9$ for t-Se). If one requires that the FE model should fulfill the translation symmetry exactly, eigenstates are still plane waves (PW), but occupation is defined by the nth BZ (nBZ).[26] This we call the translationally invariant FE (TIFE) model and obtain the result

$$B(\vec{t})=2\Omega_0/(2\pi)^3\int_{\Omega_{n\mathrm{BZ}}} d^3k\cos(\vec{k}\cdot\vec{t}) \tag{4}$$

$$=2\Omega_0/(2\pi)^3\sum_{i=1}^{m}\int_{\Omega_{n\mathrm{BZ}}} d^3k\cos(R_i\vec{k}\cdot\vec{t})\,, \tag{5}$$

where Ω_0 denotes the unit-cell volume, R_i a rotation element of the rotation group of the BZ's, and m the number of R_i's. Thus only the contribution of the irreducible part of nBZ has to be determined. The integral may always be decomposed into contributions from triangular pyramids, with the tip at $\vec{k}=0$ and the base on a face of the nBZ, each of which can be evaluated analytically. Results for the TIFE model are thus exact, unless an error in determining the nBZ is made, a task far from trivial (for t-Se the irreducible $\frac{1}{24}$ part of 9BZ has 42 faces[27]). The relation $B(\vec{T})=2n\delta_{\vec{T},0}$ provides, however, a useful check.

Neither of the above FE models fulfills the orthogonality requirement to the core, which is a serious defect for momentum space quantities, since orthogonalization introduces high-momentum components into the CP. The orthogonality may be achieved by using orthogonalized plane waves (OPW) instead of PW's. We call the result the orthogonalized-TIFE (OTIFE) model and discuss details of it in the appendix. For OTIFE, one obtains three contributions to $B(\vec{t})$. These are the PW, the PW core, and the core-core parts. Only the last contribution has an angular dependence differing from that of the PW part and thus affects the anisotropy of $B(\vec{t})$. For absolute values all terms are of course important.

Structural disorder effects are discussed using a one-dimensional potential array model.[13] The potentials are square wells chosen such that each has only two bound states, one symmetric and the other antisymmetric, to simulate the behavior of three-dimensional s and p states. Finite, infinite,

ordered, and disordered arrays may be studied with the transfer matrix formalism and results are essentially exact, since most of the calculational steps are performed analytically.

IV. RESULTS FOR TRIGONAL Se

The CP of *t*-Se along the *c* axis from the HMI and UDO experiments and the SCOPW theory is listed in Table I.[28] The RHF model gives a $1s$-$3d$ core contribution to $J(0)$ of 9.189 a.u. The SCOPW theory was convoluted both with the HMI resolution (FWHM 0.41 a.u.) and the UDO resolution (FWHM 0.65 a.u.), respectively. To be comparable with the UDO-profiles the $1s^2$ core contribution to the SCOPW theory was subtracted from the theoretical profiles. The $1s$ binding energy of Se (12.655 keV) is larger than the energy transfer of 11.2 keV corresponding to the UDO experimental CP maximum.

In all cases the theoretical CP is by 1.5—2 % above the experimental CP at the profile maximum. A profile too high for small momenta seems to be typical for all noncorrelated self-consistent calculations.[29] Taking into account the resolution effects the experimental profiles of HMI are in good overall agreement with the UDO result.

The characteristic anisotropy of the CP (ACP), as obtained from both the HMI and the UDO experiment, is given in Fig. 1, in comparison with the result of the SCOPW calculation. Experimental and theoretical data agree within the error bars except for low momenta ($q < 0.3$ a.u.), where the SCOPW ACP is significantly outside the statistical error bars. A possible explanation for this discrepancy is provided by the exchange-correlation scaling effect, which for the closely related *t*-Te lowers the ACP for small momenta considerably.[30]

TABLE I. Compton profile $J_{\vec{k}}(q)$ for trigonal Se with $\vec{k}$ parallel and perpendicular (*a* axis) to the *c* axis. J and q are in a.u., i.e., a_0 and a_0^{-1}, respectively, and J is normalized for $(-\infty, \infty)$ to 102. Experimental results are from the Hahn-Meitner-Institut (HMI) and University Dortmund (UDO). They are corrected to multiple scattering and include momentum resolution effects [full width at half maximum (FWHM) 0.41 a.u. for HMI and FWHM 0.65 a.u. for UDO]. For the theoretical SCOPW results a RHF core was used ($1s^2 2s^2 2p^6 3s^2 3p^6 3d^{10}$ for HMI and $2s^2 2p^6 3s^2 3p^6 3d^{10}$ for UDO). The theoretical results are convoluted with the HMI and the UDO resolution, respectively.

	q [001]				$J_{\vec{k}}(q)$ [100]			
	HMI *t*-Se	SCOPW HMI resol.	UDO *t*-Se	SCOPW-$1s^2$ UDO resol.	HMI *t*-Se	SCOPW HMI resol.	UDO *t*-Se	SCOPW-$1S^2$ UDO resol.
0.0	20.12±0.06	20.55	19.54±0.1	19.88	19.89	20.16	19.25	19.60
0.2	19.64	20.11	19.12	19.44	19.42	19.78	18.94	19.21
0.4	18.47	18.72	18.08	18.16	18.36	18.59	17.86	18.04
0.6	16.50	16.58	16.29	16.23	16.48	16.56	16.20	16.18
0.8	14.00	14.09	14.29	13.98	13.92	14.04	14.21	13.97
1.0	11.74±0.05	11.67	12.32	11.83	11.81	11.71	12.32	11.86
1.2	10.08	9.86	10.57	10.11	10.20	10.06	10.72	10.21
1.4	9.091	8.85	9.43	8.95	9.296	9.06	9.46	9.10
1.6	8.345	8.28	8.54	8.23	8.425	8.40	8.52	8.33
1.8	7.834	7.85	7.85	7.72	7.879	7.89	7.86	7.78
2.0	7.395±0.04	7.44	7.22±0.06	7.29	7.395	7.45	7.20	7.31
2.2	6.927	7.03	6.79	6.87	6.917	7.03	6.86	6.88
2.4	6.558	6.60	6.42	6.45				
2.6	6.120	6.18	6.05	6.03				
2.8	5.758	5.75	5.75	5.61				
3.0	5.376±0.03	5.33	5.31	5.20				
3.4	4.655	4.58	4.50	4.45				
3.8	3.966	3.93	3.76	3.80				
4.2	3.409	3.38	3.21	3.25				
4.6	2.947	2.91	2.80	2.77				
5.0	2.566±0.025	2.52	2.50±0.04	2.40				

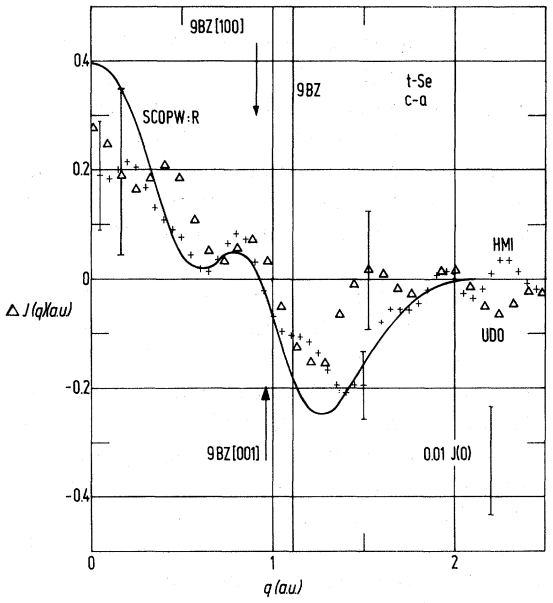

FIG. 1. Anisotropy of the Compton profile $\Delta J(q)$ for t-Se between the c and a axis. Units and normalization is as in Table I. 9BZ [001], 9BZ [100], and 9BZ denote the extent of the 9BZ in the directions [001], [100], and the direction of maximum extent, respectively. The convoluted SCOPW result (SCOPW:R) ($q=0.41$ a.u.) is given by the full line and the experimental result from HMI by the crosses, and from UDO by the triangles. Bars denote the statistical accuracy and the size of the plot. Samples t-Se [001] and t-Se [100] were used.

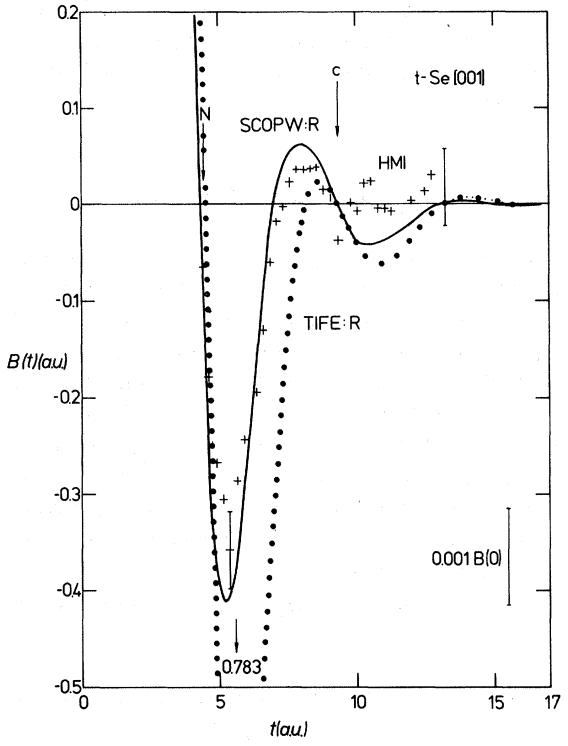

FIG. 2. Autocorrelation function $B(t)$ of the one-electron density matrix for t-Se along the c axis. B and t are in a.u., i.e., 1 denotes the Bohr radius. The norm is $B(0)=102$. N denotes the nearest-neighbor separation and c the lattice translation. The experimental result (HMI) is given by the crosses, the convoluted SCOPW result by full line, and the convoluted TIFE result by the dotted curve. The arrow and 0.783 show the location and depth of the TIFE minimum. Bars indicate the size of the statistical accuracy and the size of the plot with respect to $B(0)$. The sample t-Se [001] was used.

The long-range part of the AF for t-Se along the c and a axes is given in Figs. 2 and 3, respectively. The experimental result (HMI) (Ref. 31) is well reproduced by the SCOPW AF within statistical accuracy and is in reasonable agreement within the approximate relationship between the crystal structure and the zeros of $B(\vec{t})$ (other than translation zeros) as discussed earlier.[10] With the currently achievable momentum resolution of γ-ray Compton spectrometers and the small sample size, which limits the statistical accuracy, essentially no information may be obtained from the region beyond c (or a). The TIFE model is also seen to reproduce the structure of the experimental $B(\vec{t})$ qualitatively in the range $5 \lesssim t \lesssim 15$ a.u., but the quantitative differences in the amplitudes and positions of the zeros are large. The first minimum is in both directions too deep by a factor of 2. At distances at about a the difference between the TIFE and experiment is of the order of twice the statistical error bar. Recently it has been concluded for the tetrahedral semiconductors, that the zeros of $B(\vec{t})$ are mainly the property of the Bravais lattice and the number of occupied bands.[26] This does not apply to the anisotropic t-Se (Table II). The first zero in the TIFE results is about 0.3 a.u. shifted to higher distances as compared to the experiment (HMI) as well as the SCOPW result. The discrepancy of the positions of the second zeros in the [001] direction is still larger. (In the [100] direction the second zero is a lattice zero, and this is built in to the TIFE and the SCOPW results,

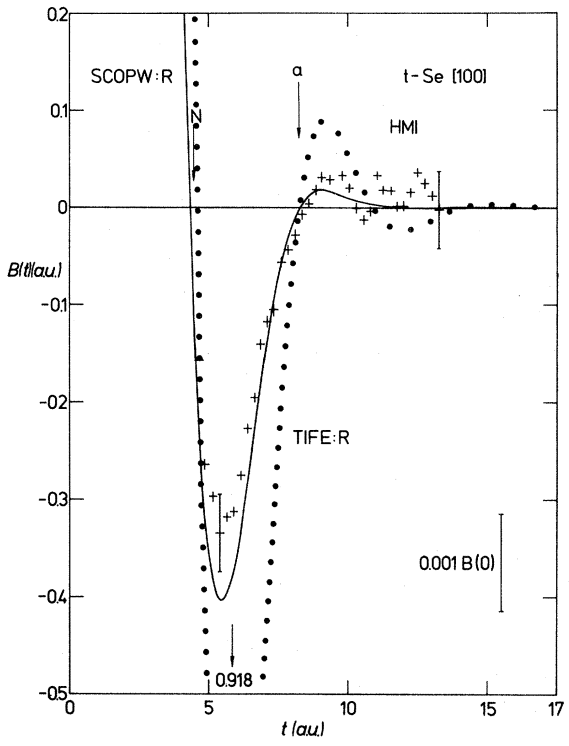

FIG. 3. Autocorrelation function $B(t)$ for t-Se along the a axis. For additional information see caption of Fig. 2. The sample used is t-Se [100] (HMI).

respectively.) The behavior of the free-electron gas traces back to the already rather spherical 9BZ, for which all 141 corners[32] of the irreducible wedge fall into the range $0.909 < q < 1.112$ a.u. Therefore, the zero positions of $B(\vec{t})$ are in general, except for the lattice zeros of course, influenced by ion-ion, electron-ion, and electron-electron interactions as described by an effective crystal potential, and not only an expression of the translation symmetry and the occupation of the Brillouin zones. Expressed in terms of a more chemical language coordination, type of orbitals, and orthogonalization are the important factors here. Evidently the rather high-symmetry constraints on the AF together with the low number of atoms per unit cell play an important role in the case of the tetrahedral crystals Si and Ge.

The anisotropy of $B(\vec{t})$ is displayed in Fig. 4. The experimental result (HMI) and the SCOPW model again agree well within the resolution and the statistical accuracy. The theoretical model shows, however, a consistently slightly larger anisotropy, an effect which has been found also in other first-principles calculations for covalent semiconductors.[33,34] The TIFE model provides a simple interpretation of some of the structure of this anisotropy. The two broad peaks in the range $5 < t < 13$ a.u., also present in the TIFE result, are basically determined by *structural* effects, i.e., translation symmetry and BZ occupation, although crystal potential effects tend to reduce the anisotropy. However, for $t < 5$ a.u. there is a drastic discrepancy between the TIFE model and both the experiments and the SCOPW result. Corrections to the TIFE model from core orthogonalization may be discussed using the OTIFE variant. The analysis given in the Appendix indicates that core orthogonalization does not change the sign of the anisotropy of $B(\vec{t})$ for small values of t and the core orthogonalization effect may thus be ruled out for the explanation of this discrepancy. It is instructive to decompose the TIFE result into triplet contributions in order to trace back the origin of the anisotropy of $B(t)$ at $t=3$ a.u. Figure 5 displays the cumulative triplet contributions to the AF anisotropy from the 3BZ, 6BZ, and 9BZ. In this picture 1BZ—3BZ corresponds to the s-like triplet, 4BZ—6BZ to the bonding p-like triplet, and 7BZ—9BZ to the nonbonding lone-pair triplet in the band structure of Se.[11,25] Evidently the 4BZ—6BZ, corresponding to the intrachain bonding triplet, is responsible for the large negative

TABLE II. Distances between nth neighbors in trigonal Se, d_n, as compared to the positions of the zeros in $B(t)$, t_n, parallel [001] and perpendicular [100] to the chains in a.u.

		t_n [001]			t_n [100]		
n	d_n	HMI	SCOPW	TIFE	HMI	SCOPW	TIFE
1	4.48	4.40	4.32	4.54	4.36	4.33	4.60
2	7.02	7.35	7.02	8.17			
3	8.25				8.5	8.28	8.25
4	9.36	9.0	9.32	9.35			

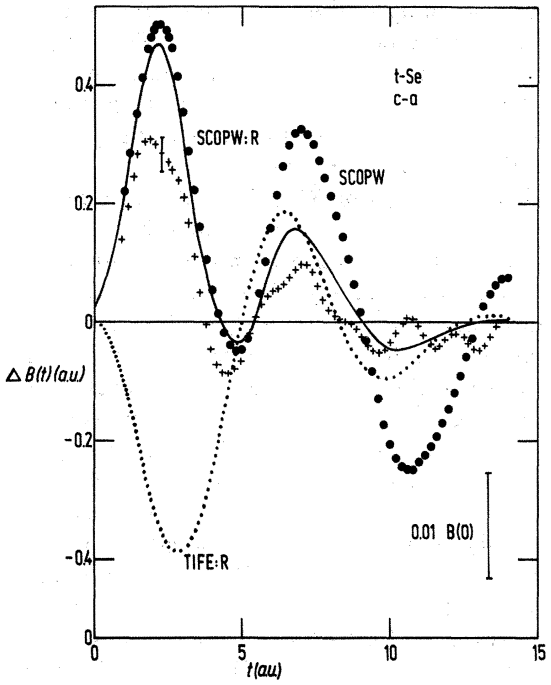

FIG. 4. Anisotropy of the autocorrelation function $\Delta B(t)$ for t-Se for the difference c-a axis. Units, norm, and curves as in Fig. 2. Full circles denoted by SCOPW represent the unconvoluted results as obtained from the SCOPW calculation.

peak in the anisotropy of $B(t)$ as resulting from the TIFE model at distances $t \lesssim 5$ a.u. Neither hybridization nor self-consistent effects are included in the TIFE. Thus, one may conclude that the positive peak in the experimental anisotropy arises mainly from the intrachain bonding interactions. A similar positive peak in the anisotropy of the AF has been observed in orthohombic sulfur,[35] which has a different crystal structure though its valence-electron configuration is the same. A quantitative explanation in the language of the chemical bond is, however, only possible by performing a linear combination of atomic orbitals calculation or by a direct comparison with the SCOPW results for individual band contributions, as already performed for the momentum densities.[11]

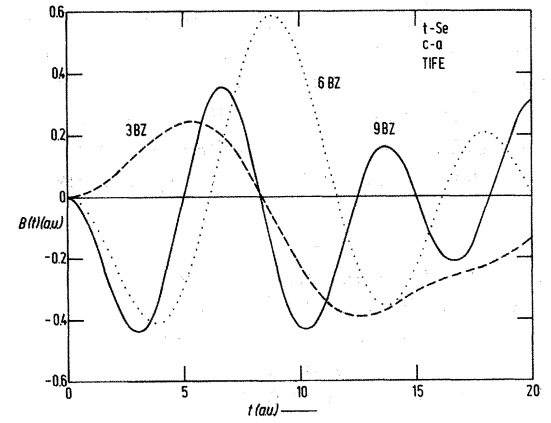

FIG. 5. Cummulative Brillouin-zone contributions to the anisotropy of the autocorrelation function $\Delta B(t)$ for t-Se for the difference c-a axis. Results for the TIFE model from 3BZ, 6BZ, and 9BZ are given by the dashed curve, dotted curve, and full curve, respectively.

V. POLYCRYSTALLINE Se

The experimental AF for polycrystalline trigonal Se (pct-Se) together with a number of model results is plotted in Fig. 6. The atomic RHF AF corresponds to the configuration $4s^2 4p^4$ and has been derived from radial functions only without any crystal-field effects. It has been shown earlier[13] that $B(t)$ is dominated by the local arrangement of atoms in relatively small clusters. It converges rapidly with the size of the cluster and performs a structural average over the configurations of atom clusters in the material. Therefore, an angular average AF of the single crystal should give a reasonable description of the AF of the polycrystalline material. The simplest average for pct-Se includes only the directions c and a with weights $\frac{1}{3}$ and $\frac{2}{3}$. The resulting averages both for the SCOPW and TIFE models are also shown in Fig. 6. The same average over the intrachain and interchain next-nearest-neighbor separations, 7.023 and 8.251 a.u., respectively, also coincides with the second zero of $B(t)$ (Fig. 6). The averaged TIFE result is quantitatively similar to that of the spherically symmetric FE model, with the first zeros of $B(t)$ within 0.7%, and the second zeros within 5.1%, although the amplitudes for FE are consistently larger. The experimental AF is in agreement with the averaged SCOPW model within the statistical accuracy, and confirms the averaging concept.

It is interesting to see whether the monoclinic (α and β) phases of Se (m_α-Se and m_β-Se) may be distinguished from t-Se in the Compton experiment. Because of problems associated with crystal growth only polycrystalline monoclinic Se (pcm-Se), including m_α-Se and m_β-Se roughly in equal amounts, has been studied. Characteristic structur-

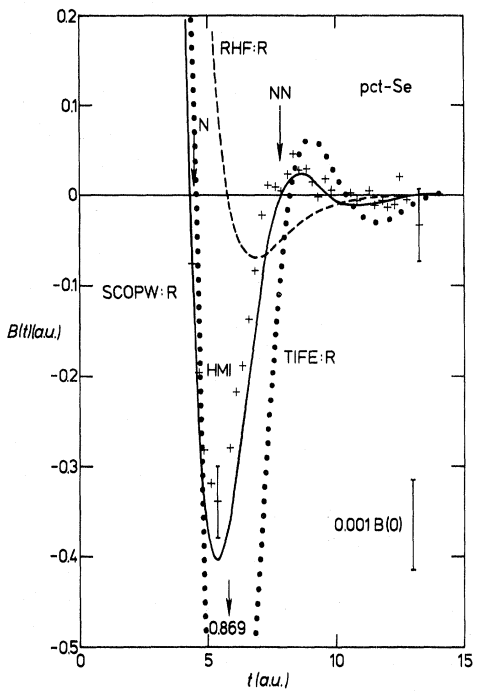

FIG. 6. Autocorrelation function $B(t)$ for pct-Se. Units, norm, statistical accuracy, and size of plot are given as in Fig. 2. N denotes the nearest-neighbor separation and NN the average next-nearest-neighbor separation. The experimental result for sample pct-Se_{II} (HMI) is given by the crosses, the convoluted SCOPW result by the full line, the convoluted TIFE AF by the dotted line, and the convoluted RHF profile by the dashed line. The TIFE minimum outside the plot area is given earlier.

al parameters influencing the chemical bond are, however, very similar for t-Se and m-Se (Ref. 36): the average nearest-neighbor separations, the average next-nearest-neighbor separations (within the same chain or ring), and the interchain and inter-ring nearest-neighbor separations are 4.48, 7.02, and 6.49 a.u. for t-Se; 4.42, 7.03, and 6.67 a.u. for m_α-Se; and 4.42, 7.04, and 6.58 a.u. for m_β-Se, respectively. Also the mean density, as expressed by the Fermi momentum p_F with values 0.988, 0.960, and 0.956 a.u. for t-Se, m_α-Se and m_β-Se, respectively, is almost the same. Thus, any differences that may be present in the AF result, mainly can arise from differences in the inter-ring and interchain or the intraring and intrachain second-neighbor interactions. The experimental result is given in Fig. 7. There is no phase difference substantially larger than the statistical error. The analysis of the small difference in the range

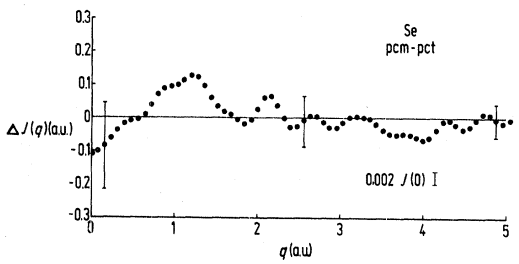

FIG. 7. Difference of the experimental Compton profiles $J(q)$ (UDO) between the polycrystalline monoclinic and polycrystalline trigonal Se given by pcm-pct. J and q are in a.u. Norm is $B(0)=102$.

$0<q<1.2$ a.u. by Fourier transforming the difference curve of Fig. 7 gives a strong indication for differences in multiple scattering (differences in the AF for $0<t<0.5$ a.u.), which can arise from different sample thickness. Therefore, no further theoretical analysis has been performed.

VI. AMORPHOUS Se

At least two amorphous phases of Se are known to exist, namely black amorphous Se (ba-Se) and red amorphous Se (ra-Se). The latter undergoes a slow phase transition below 303 K into m-Se and above 303 K into t-Se.[37] Since Se is twofold coordinated, the short-range order (SRO) in the amorphous phases of Se must be based on rings and chains of atoms in varying proportions. Diffraction studies[38–40] and photoemission[41,42] suggest

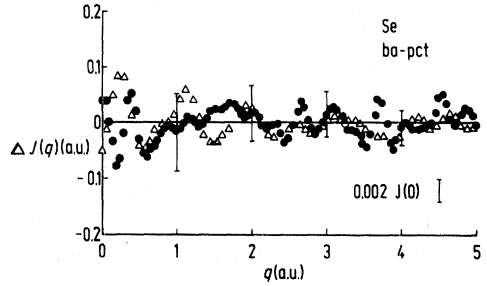

FIG. 8. Difference of Compton profiles $\Delta J(q)$ of black amorphous and polycrystalline trigonal Se in that order. J and q are in a.u. Norm is $B(0)=102$. The samples ba-Se_{II} and pct-Se_{II} have been used. The dots are the results from the HMI spectrometer, the triangles from UDO. The statistical accuracy of the HMI results is indicated by the bars. The UDO error bars are about 1.5 larger.

that the network topology depends on sample preparation. Extended x-ray absorption fine structure (EXAFS) gives no information on the SRO beyond nearest neighbors.[43] Infrared (ir) and Raman results are currently also interpretated such that the SRO alternates locally between chainlike (*cis*) and ringlike *(trans)* configurations.[44]

The experimental result for the difference of the CP's of ba- and pct-Se is given in Fig. 8. Neither the HMI nor the UDO spectrometer detected any statistically significant difference in $\Delta J(q)$. According to our model studies no difference is seen in the CP if the SRO averages in the ordered and disordered phases are the same.[13] This condition should be fulfilled for Se, since chain- and ringlike regions differ from each other only beyond the second neighbors, when measured with their SRO averages. The present experimental result is fully compatible with previous information on the SRO in ba-Se. In order to see effects up to third neighbors the momentum resolution must be improved.

VII. DISCUSSION

The three characteristic quantities describing the quality of a Compton experiment are the width (FWHM), Δq of the momentum resolution function $R(q)$, the statistical accuracy $\sigma(q)$ of the counting process, and the ratio of the number of valence electrons n_v, to the total number of electrons n_t. Via the convolution theorem the momentum resolution Δq corresponds to the position resolution (FWHM) $\Delta t = 8\ln 2/\Delta q$ of the associated multiplicative resolution function $R(t)$.

The present values for $\Delta q = 0.41$ and 0.56 a.u. for HMI and UDO, respectively (Sec. II), have to be compared with p_F, which for all phases of Se has a value of about 1 a.u. The relation to structural details is more evident in position space, where the effect of $R(t)$ is to reduce the signal by a factor of 2 at 6.7 and 4.9 a.u., respectively. The relative statistical accuracy for the HMI spectrometer and Se is about $\sigma(0)/J(0) \simeq 0.003$ for the CP or $\sigma(0)/B(0) \simeq 0.0003$ for the AF. For anisotropies and phase differences one is studying differences in the n_v/n_tth part of the total signal. For Se this means, unfavorably, $n_v/n_t \sim 0.2$. The combined effect of these factors is such that for Se absolute profiles for $B(t)$ may be measured approximately in the range $0 < t < 9$ a.u. with relative statistical error bars of the order of $2\sigma/B(0) \simeq 0.0006$. For difference profiles no universal relative accuracy may be given, because there is no *a priori* reference quantity. For the anisotropy of, e.g., *t*-Se, we have $2\sigma/\max(\Delta B) \simeq 0.2$.

Consider then the crystalline and polycrystalline phases of Se first. In all cases both the SRO and the long-range order (LRO) are well known from elastic scattering and hence electronic effects may be separated. For *t*-Se the relation between the structural and electronic contributions is best understood using the SCOPW model. SRO and LRO effects influence the behavior of absolute and difference CP's for all values of q, whereas a separation is possible in position space. A modest qualitative representation of the absolute AF's may well be obtained by any free-electron-like model fulfilling only LRO requirements, but especially for correlation lengths not larger than the second-neighbor separation, the induced errors are as large as one order of magnitude. Quantitatively correct anisotropies, on the other hand, require both bonding and LRO information, whereas for qualitatively correct anisotropies, hybridization and orthogonality of the bond orbitals up to nearest-neighbor interaction may be sufficient. Generally, for distances below second neighbors of the same structural unit, bonding effects are dominant for covalent solids, and beyond the second neighbor, the LRO is the significant factor. The polycrystalline averages for pct-Se and pcm-Se obey essentially the same rules. Since the SRO averages in both cases are very close to each other up to second neighbors (Sec. V), differences between different crystal phases must be extremely small quantitative effects.[13] This is exactly what has been seen in the present experiments.

It was shown that ba-Se and pct-Se have almost the same $B(t)$ up to second-neighbor distances. It may be concluded from the model studies performed for ordered and disordered one-dimensional chains[13] that the corresponding SRO averages and electron states in this range are very much similar indeed. The quantitative features of $B(t)$ also depend on interactions from farther neighbors. Therefore, an admixture of, for instance, regions in ba-Se with Se-ring molecules might be expected to be detectable (also the nearest-neighbor separation is slightly smaller for the ringlike structures). This would be equivalent to differences in the average SRO above third-neighbor distances. Since, within the present experimental accuracy, it is not possible to detect differences in $B(t)$ between the various phases for $t \gtrsim 9$ a.u., we cannot conclude anything about structural properties and the features of the

electronic states beyond the second-neighbor distance. Thus, Compton spectroscopy yields information on the SRO and the chemical bond in the various phases of Se which is consistent within the results of x-ray diffraction, photoemission, EXAFS, and ir and Raman spectroscopy. However, at present only instrumental and not fundamental factors limit the resolution. A better performance, in order to widen the range for probing the SRO, the electronic wave functions, and correlation effects, is, at least in principle, achievable.

ACKNOWLEDGMENTS

Two of the authors (P.K. and B.K.) acknowledge interesting discussions with Angus MacKinnon. One of the authors (P.K.) expresses his gratitude for hospitality at the Physikalisch-Technische Bundesanstalt in the final phase of this work. This work was supported by the Deutsche Forschungsgemeinschaft.

APPENDIX: THE ORTHOGONALIZED TIFE MODEL

The orthogonalized plane wave (OPW) $|X_{\vec{k}}\rangle$ is obtained from the PW $|\vec{k}\rangle$ using the valence projector $Q_{\vec{k}}$,

$$|X_{\vec{k}}\rangle = Q_{\vec{k}}|\vec{k}\rangle = \left(1-\sum_{qnlm}|qnlm\vec{k}\rangle\langle qnlm\vec{k}|\right)|\vec{k}\rangle , \tag{A1}$$

where the core state $|qnlm\vec{k}\rangle$ is labeled with a unit-cell atom index q, and the standard set of quantum numbers n, l, and m.

Since, however, $\langle X_{\vec{k}+\vec{G}}|X_{\vec{k}'+\vec{G}'}\rangle=0$, where $\vec{G}$ and $\vec{G}'$ denote reciprocal lattice vectors, only if the reduced wave vectors $\vec{k}$ and $\vec{k}'$ are unequal, one has to orthogonalize for each reduced wave vector $\vec{k}$ all $|X_{\vec{k}}\rangle$'s belonging to the nBZ's. We do not want to elaborate on this further here, but consider instead for qualitative purpose the orthogonalized TIFE (OTIFE) model, which fulfills this latter requirement only approximately. The relation $B(\vec{T})=2n\delta_{\vec{T},0}$ is not violated by this. Instead of Eq. (4) we then obtain

$$B(\vec{t})=2\frac{\Omega_0}{(2\pi)^3}\int_{\Omega_{nBZ}}d^3k\left[1-\frac{4\pi}{\Omega_0}\sum_{qnl}(2l+1)(b^q_{nlk})^2\right]^{-1}\times\left[e^{-i\vec{k}\cdot\vec{t}}\left[1-\frac{8\pi}{\Omega_0}\sum_{qnl}(2l+1)(b^q_{njk})^2\right]+\frac{(4\pi)^2}{\Omega_0}\sum_{\substack{qnlm\\q'n'l'm'}}e^{i\vec{k}\cdot(\vec{\tau}_q-\vec{\tau}_{q'})}i^{l*}i^{l'}Y_l^m(\theta_{\vec{k}},\phi_{\vec{k}})^*Y_{l'}^{m'}(\theta_{\vec{k}},\phi_{\vec{k}})b^q_{nlk}b^{q'}_{n'l'k}S_{qnlm\vec{k},q'n'l'm'\vec{k}}(\vec{t})\right], \tag{A2}$$

where the orthogonalization coefficient is defined as

$$b^q_{nlk}=\int_0^\infty dr\, j_l(kr)R^q_{nl}(r)r^2 , \tag{A3}$$

and the core state $|qnlm\vec{k}\rangle$ AF as

$$S_{qnlm\vec{k},q'n'l'm'\vec{k}}(\vec{t})=\int_\Omega d^3r\langle\vec{r}|qnlm\vec{k}\rangle\langle q'n'l'm'\vec{k}|\vec{r}+\vec{t}\rangle . \tag{A4}$$

All other notation has the usual meaning.[24] For $b^q_{nlk}=0$, Eq. (A2) reduces to Eq. (5).

Corrections to the TIFE model from orthogonalization may be discussed with reference to Eq. (A2), which contains valence-valence, valence-core, and core-core terms in the square brackets, respectively. Since the first two contributions (in large parentheses) have the same angular dependence, only the core-core terms may affect the sign of the anisotropy. For the core state AF one finds for $\vec{t}=\vec{T}$

$$S_{qnlm\vec{k},q'n'l'm'\vec{k}}(\vec{T})=\delta_{qq'}\delta_{nn'}\delta_{ll'}\delta_{mm'}e^{-i\vec{k}\cdot\vec{T}} .$$

Here $\vec{T}$ is a lattice translation. The associated m sum can then be carried out and the whole integrand reduces to $e^{-i\vec{k}\cdot\vec{T}}$. Since the core function AF is a smooth function for small $\vec{t}$ for all $|qnlmk\rangle$, we conclude that core orthogonalization effects do not change the sign of the anisotropy of the TIFE model for small $\vec{t}$.

[1]For a recent review see *Compton Scattering*, edited by B. G. Williams (McGraw-Hill, New York, 1977).

[2]P. M. Platzman and N. Tzoar, Phys. Rev. 139, A410 (1965).

[3]P. Eisenberger and P. M. Platzman, Phys. Rev. A 2, 415 (1970).

[4]See, e.g., P. Kaijser and V. H. Smith, Jr., Adv. Quantum Chem. 10, 37 (1977).

[5]See, e.g., W. Weyrich, *Habilitationsschrift* (Technische Universität Darmstadt, Darmstadt, 1978); W. Weyrich, Ber. Bunsenges. Phys. Chem. 83, 797 (1979).

[6]K. F. Berggren, S. Manninen, T. Paakkari, O. Aikala, and K. Mansikka, in *Compton Scattering*, edited by B. G. Williams (McGraw-Hill, New York, 1977), p. 139.

[7]U. Bonse, W. Schröder, and W. Schülke, Solid State Commun. 21, 807 (1977).

[8]P. Krusius, B. Kramer, O. Schütz, and J. Treusch, Solid State Commun. 21, 1127 (1977).

[9]B. Kramer and P. Krusius, Phys. Rev. B 16, 5341 (1977).

[10]B. Kramer, P. Krusius, W. Schröder, and W. Schülke, Phys. Rev. Lett. 38, 1227 (1977).

[11]P. Krusius, J. Phys. C 10, 1875 (1977).

[12]R. Kaplow, T. A. Rowe, and B. L. Averbach, Phys. Rev. 168, 1068 (1969).

[13]P. Krusius, H. Isomäki, and B. Kramer, Phys. Rev. B 19, 1818 (1979).

[14]R. J. Weiss, W. A. Reed, and P. Pattison, in *Compton Scattering*, edited by B. Williams (McGraw-Hill, New York, 1978), pp. 43–78.

[15]P. Pattison and J. R. Schneider, Nucl. Instrum. Methods 158, 145 (1979).

[16]M. Cooper, P. Pattison, and J. R. Schneider, Philos. Mag. 34, 243 (1976).

[17]F. Biggs, L. B. Mendelsohn, and J. B. Mann, At. Data Nucl. Data Tables 16, 201 (1975).

[18]J. Felsteiner and P. Pattison, Phys. Rev. B 13, 2702 (1976).

[19]U. Bonse, W. Schröder, and W. Schülke, J. Appl. Crystallogr. 12, 432 (1979).

[20]E. Clementi and C. Roetti, At. Data Nucl. Data Tables 14, 177 (1974).

[21]R. C. Keezer and C. Wood, Appl. Phys. Lett. 8, 139 (1966).

[22]The *t*-Se crystals were supplied by M. Meissner of the Fritz-Haber-Institut, Berlin.

[23]J. W. Moody and R. C. Hines, Mater. Res. Bull. 2, 523 (1967).

[24]J. von Boehm and P. Krusius, Int. J. Quantum Chem. VIII, 395 (1974).

[25]P. Krusius, J. von Boehm, and T. Stubb, Phys. Status Solidi B 67, 551 (1975).

[26]A. MacKinnon and B. Kramer, J. Phys. C 13, 37 (1980).

[27]A face is here defined such that all angles of the limiting polygon on the associated plane are less than 180°.

[28]Lattice parameters are from P. Unger and P. Cherin, *The Physics of Selenium and Tellurium*, edited by C. Cooper (Pergamon, New York, 1967).

[29]See, e.g., L. Mendelsohn and V. H. Smith, Jr., in *Compton Scattering*, edited by B. G. Williams (McGraw-Hill, New York, 1977), p. 102.

[30]Exchange-correlation scaling effects within the local density formalism have not been studied for Se because of the enormous computer expenses associated. However, data exist for trigonal Te, which has a very similar ground state. From Figs. 4–6, in P. Krusius, T. Stubb, H. Isomäki, and J. von Boehm, Phys. Rev. B 22, 2955 (1980), it can be deduced that exchange-correlation scaling has an effect of the order of 1.5% on $J(0)$. This is roughly 50% of the anisotropy $\Delta J(0)$. For $q\neq 0$ the effect is always smaller.

[31]The corresponding UDO results are in a good overall agreement with the experimental HMI AF's but were not displayed in the Figs. 2–4 and 6 since their statistical accuracy (depending on the total number of counts) is by a factor 1.5–2.5 lower than that of the HMI experiment. Thus, their representation would overload the figures and lead to confusion.

[32]All corner points of the polygon faces of the irreducible wedge of the 9BZ are included into this number. Since each point is shared by at least three faces the actual number of different points is roughly one third of this.

[33]G. G. Wepfer, R. N. Euwema, G. T. Surratt, and D. L. Wilhite, Phys. Rev. B 9, 2670 (1974).

[34]A. Zunger and A. J. Freeman, Phys. Rev. B 15, 5049 (1977).

[35]K. D. Petri, A. MacKinnon, B. Kramer, and P. Krusius, Solid State Commun. 36, 833 (1980).

[36]R. W. G. Wyckoff, *Crystal Structures* (Interscience, New York, 1960).

[37]G. Gobrecht, G. Willers, and D. Wobig, Z. Phys. Chem. Neue Folge 77, 197 (1972).

[38]J. C. Malaurent and J. Dixmier, in *The Structure of*

Non-Crystalline Materials, edited by P. H. Gaskell (Taylor and Francis, London, 1977), p. 49.

[39]A. I. Andrievskii, I. D. Nabovich, and Ya. V. Voloschuk, Kristallografiya 5, 369 (1960) [Sov. Phys.—Crystallogr. 5, 349 (1960)].

[40]M. D. Rechtin and B. L. Averbach, J. Non-Cryst. Solids 12, 391 (1973); Solid State Commun. 13, 491 (1973).

[41]B. Kramer, K. Maschke, and L. D. Laude, Phys. Rev. B 8, 5781 (1973); and L. D. Laude, B. Kramer, and K. Maschke, *ibid.* 8, 5794 (1973).

[42]T. Takahashi, K. Ohno, and Y. Harada, Phys. Rev. B 21, 3399 (1980).

[43]T. M. Hayes and S. H. Hunter, in *The Structure of Non-Crystalline Materials,* edited by P. H. Gaskell (Taylor and Francis, London, 1977), p. 69.

[44]See, e.g., G. Lucovsky, in *The Physics of Selenium and Tellurium,* edited by E. Gerlach and P. Grosse (Springer, Berlin, 1979).